Qualitative Properties of Solutions to Systems of Fokker-Planck Equations for Multilane Traffic Flow

M. Herty * R. Illner† A. Klar ‡ V. Panferov§

April 30, 2004

Abstract

A review of recently introduced Fokker-Planck-type systems of partial differential equations as kinetic models of multilane traffic flow is given, and we present a series of analytical and numerical studies for these models. In particular, we investigate the convergence to equilibria, explain why equilibria of the present models may show jump discontinuities at the average speed, and explore synchronization on adjacent lanes from both an analytical and numerical point of view. Finally, we present numerical studies which explain the formation and propagation of stop-and-go waves.

*FB Mathematik, TU Darmstadt, Schlossgartenstr.7, 64289 Darmstadt, Germany, (herty@mathematik.tu-darmstadt.de).

†Department of Mathematics and Statistics, University of Victoria, P.O. Box 3045, Victoria, B.C. V8W 3P4, Canada, (rillner@math.uvic.ca).

‡FB Mathematik, TU Darmstadt, Schlossgartenstr.7, 64289 Darmstadt, Germany, (klar@mathematik.tu-darmstadt.de).

§Department of Mathematics and Statistics, University of Victoria, P.O. Box 3045, Victoria, B.C. V8W 3P4, Canada, (panferov@math.uvic.ca).

Contents

1 Introduction

We are concerned with systems of Fokker-Planck type equations as introduced in Ref. [6] as kinetic models for traffic flow in a multilane freeway. For other kinetic traffic flow models, see for example [15, 14, 13, 10, 11, 4]. Some analytical results on the asymptotic behaviour of solutions of these equations in the spatially homogeneous case were obtained in [5] where the applicability of entropy methods was explored.

In the case of two lanes the system of equations under consideration is

$$\partial_t f_i + v\partial_x f_i + \partial_v(B[f](t,x,v)f_i - D[f]\partial_v f_i) = p_k[f]f_k - p_i[f]f_i \quad (1.1)$$

$$(t,x,v) \in \mathbb{R}^+ \times \mathbb{R} \times [0, u_{\max}] \quad (1.2)$$

$$i = 1,2, \quad k = 3-i, \quad (1.3)$$

where the braking and acceleration terms (abbreviated as $B[f]$) depend on lane-changing probabilities; these probabilities are assumed to depend in simple (but non-local!) ways on the macroscopic traffic density and flux. Moreover, there are lane-changing terms on the right-hand sides of the equations, and there is a (degenerate) diffusion term in each equation, justified by the inability of the average driver to accurately estimate average speeds ahead. We present the details of the model in Section 2 below.

Here we explore qualitative properties of these systems from both analytical and numerical points of view. First, we conduct a discussion concerning the various modeling assumptions made in [6] and offer suggestions for generalizations. This is done in Section 2. There we review the definitions of the braking, acceleration and diffusion terms. Some comments regarding the definition of more realistic lane-change probabilities are given. We also investigate the consequences of the degeneracy of the diffusion term D and explain the occurrence of discontinuous equilibria, observed originally (and unexpectedly) in the numerical experiments presented in Section 3. The diffusion term D, as defined in [6], is $D = \sigma(\rho, u)|v-u|^\gamma$, and the degeneracy at $v = u$ is obvious. As we demonstrate analytically in Section 2, and numerically in Section 3, it is this degeneracy which allows jumps at the average speed in the equilibria.

A simple way of eliminating this degeneracy is to assume a "residual" diffusion ε, active even when a driver moves exactly at the macroscopic speed as observed ahead. Thus D would become $D_\varepsilon = \sigma(\rho, u)(|v-u|^\gamma + \varepsilon)$. We consider such a modification as reasonable because drivers make inevitable small errors in judging the traffic situation ahead, even in very homogeneous traffic. The residual diffusion would prevent the model from permitting discontinuous equilibria; however, the statistically averaged traffic profile could still evolve towards, and stay for a long time, near "metastable" densities with large gradients at the average speed. That such profiles are a possibility is implicitly suggested by the asymmetry between braking and acceleration scenarios.

In Section 3 we present a series of numerical experiments regarding the qualitative behavior of solutions. Specifically, we investigate the asymptotic evolution of solutions in the spatially homogeneous scenario. As mentioned above, the system will typically converge to an equilibrium with a discontinuity at the average speed; in [6] such equilibria were not considered, as it was tacitly assumed that realistic equilibria would be continuous. This assumption would certainly be reasonable if the diffusion were never zero, i.e., if the degeneracy were to be eliminated from the model as outlined earlier.

If there is no residual diffusion, the discontinuous equilibria offer degrees of freedom towards extensions of the fundamental diagram. In particular, there may by domains in the ρ, u plane where many equilibria, most with a discontinuity, coexist. The numerical experiments in Section 3 suggest that this may be a realistic scenario.

In addition, we show simulations which confirm that the models predict synchronization of traffic on adjacent lanes. In view of the lane-changing terms on the right-hand sides of the equations, this is not surprising, but is consistent with observations made by B. Kerner [9] on the A5 in Germany. We investigated whether the synchronization could be predicted analytically, but while this seems a reachable goal, we were only able to produce a proof for a simplified model. The argument, based on a Fourier series expansion method, is presented in Section 4.

Other numerical experiments presented in Section 3 concern the familiar phenomenon of the formation of stop-and-go waves behind a bottleneck. See [7, 8] for observations and [2, 3, 12] for models exhibiting such a behaviour. We found that such waves do indeed form in suitable density regimes, and their strength and propagation was closely related to the extent drivers would look ahead. The numerical experiments also suggest that stop-and-go waves will only be predicted when the model incorporates both time lags and a multivalued fundamental diagram as explained in [6]. If the model is modified such that the fundamental diagram remains single-valued (to achieve this all one has to do is to modify the lane-change probabilities such that they do depend only on ρ and not on v, u) no stop-and-go waves formed in the numerical tests; if, on the other hand, one keeps the model with the bifurcated fundamental diagram but sets the time lags to zero, the numerical tests again showed no trace of stop-and-go waves. In summary, it appears that stop-and-go waves as predicted by the Fokker-Planck models under consideration depend on three vital ingredients: 1) a trigger, for example a lane ending and forced merging of traffic, 2) the look-ahead behaviour of drivers while braking or accelerating, and 3) a multivalued fundamental diagram. All three are consistent with traffic observations in multi-lane traffic.

2 The model

2.1 A review of the model details

We repeat the definitions of the various terms in (1.1) for the convenience of the reader. The kinetic car density at time t on lane $i = 1, 2$ per unit length and unit speed is denoted by $f_i(t, x, v)$. The macroscopic density and flux are then the zeroth and first moment of f_i :

$$\rho_i(t, x) = \int f_i(t, x, v)\ dv, \qquad j_i(t, x) = \int v f_i(t, x, v)\ dv,$$

and the average speed is $u_i = j_i/\rho_i$. When there is no dependence on the lane (such as in homogenized scenarios) we shall omit the subscript i. We assume a speed limit $v_{max} = u_{max}$, and we assume that all drivers observe this speed limit. Later we will normalize the speed limit as 1.

For the scenarios of braking (labelled by "B") and acceleration ("A") it will be assumed that there are characteristic safety distances H_X, $X = A, B$ and characteristic reaction times T_X (with $T_B < T_A$) such that the reaction of a driver at time t, position x and moving with speed v will be relative to the observed traffic at $x + H_X + T_X v$, and at time $t - \tau$, where τ is the individual reaction time.

To simplify the subsequent formulas, we define for $X = A$ or $X = B$

$$\rho^X = \rho^X(x, t) = \rho(x + H_X + T_X v, t - \tau), \tag{2.4}$$

and similarly for u^X, ρ^X and u^X also depend on v and τ, but we will suppress these dependencies in order to keep the notation simple. Note that the introduction of the safety distances is a small but reasonable change with respect to the modeling given in [6]. The values of the constants used in our numerical experiments are given in Section 3.

The braking and acceleration terms in (1.1) are given by ([6])

$$B[f](t,x,v) = \begin{bmatrix} -c_B(v-u^B)^2 q(\rho^B, u^B, v) & v > u^B \\ c_A(u^A - v)^2(\rho_{\max} - \rho^A) & v \le u^B, v \le u^A \\ 0 & \text{else} \end{bmatrix} \tag{2.5}$$

$$q(\rho,u,v) = \rho(1 - P(u,v)) \tag{2.6}$$

$$P(u,v) = \begin{bmatrix} (\frac{v-u}{u_{\max}-u})^\delta & v > u \\ 0 & \text{else} \end{bmatrix} \tag{2.7}$$

Here $P = P(u,v)$ is the lane change probability, and $1 - P$ is the braking probability. The explicit P given above is independent of ρ but is scaled to be a probability. Alternative forms of P are discussed below.

The setup of the dependencies of $B[f]$ is such that the constants c_A and c_B are dimensionless.

The ansatz for the diffusion coefficient is

$$D[f](\rho,u,v) = \begin{bmatrix} \sigma(\rho^B, u^B)|v - u^B|^\gamma & v > u^B \\ \sigma(\rho^A, u^A)|v - u^A|^\gamma & \text{else} \end{bmatrix} \tag{2.8}$$

with $\gamma \ge 1$ and where the function $\sigma(\rho, u)$ is as in reference [6]:

$$\begin{aligned} &\sigma(\rho,u) = \sigma_c \rho_{\max} u_{\max}^2 m_1(\frac{\rho}{\rho_{\max}}) m_2(\frac{u}{u_{\max}}), \\ &m_2(s) = s(1-s), \end{aligned} \tag{2.9}$$

m_1 consists of two linked Gaussian distributions and is chosen such that diffusion vanishes in the limit scenarios where $\rho = 0$ or $\rho = \rho_{\max}$. The function m_2 also is chosen such that the diffusion vanishes for $v = 0$ and $v = u_{\max}$. Finally, σ_c is positive constant to be specified later. The lane change rates $p_i[f]$ in (1.1) are

$$p_i[f](t,x,v) = \alpha j_i(t,x) P(u_i^B, v),$$

where α is a dimensionless constant, $j_i(t,x)$ is the macroscopic flux and $P(U_i^B, v)$ is the lane change probability given in (2.7).

2.2 Discussion

1. In spatially homogeneous scenarios

$$\rho^B(t,x) = \rho(t) = \rho^A(t,x), \quad u^B(t,x) = u(t) = u^A(t,x),$$

i.e., all time lags and entailed nonlocalities become irrelevant.

2. The diffusion coefficient D as given above is degenerate. In [6] this degeneracy was included intentionally, because it permits, at least when $\gamma > 1$, Dirac-Delta equilibria supported at the average speed, and such solutions are physically reasonable because "everybody could just drive at the same speed." However, as we are really discussing a statistical description of traffic scenarios, it is questionable how seriously one should take these Dirac Delta solutions. Their stability (or instability) will depend on the parameters of the system; a careful analytical study remains to be done. A side effect of the degeneracy is that even in the absence of Dirac-Delta parts to the solutions, the solutions to the spatially homogeneous equation will typically form discontinuities at the average speed, a phenomenon explained in the sequel. To avoid such discontinuities one could remove the degeneracy by replacing D by

$$D_\epsilon[f](\rho,u,v) = \sigma(\rho,u)(|v-u|^\gamma + \epsilon),$$

where ϵ is thought of as a background diffusion, active in all situations. This modification will, of course, remove the Dirac Delta and discontinuous equilibria.

3. A separate but related point is that the suggested diffusion is symmetric for $v - u > 0$ and $v - u < 0$, so braking and acceleration scenarios are assumed to give rise to the same diffusion. This is probably not realistic.

4. The lane change probability in the present model depends only on u^B on the same lane and is independent of densities altogether. This is certainly acceptable for the spatially homogeneous case, where all lanes are equivalent and the density is constant, but is clearly inadequate for the inhomogeneous case. A more realistic ansatz could be as follows: Consider a car in lane 1 (the right lane) driving with speed $v > u_1^B$. Suppose that the density and average speed on the other (left) lane as seen by the driver, possibly in his/her rear mirror, are ρ_2 and u_2. We suggest that a more realistic lane change probability function for inhomogeneous traffic is

$$P = P_2(\rho_2(u_2 - v))P_1(u_2 - u_1^B)\left(\frac{v - u_1^B}{v_{max} - u_1^B}\chi_{\{v \geq u_1^B\}}\right) \tag{2.10}$$

Here P_1 is a "lane change motivation" factor, zero for $u_2 - u_1^B < 0$, then increasing for $0 \approx u_2 - u_1^B < v_{max}$, with saturation at 1. The factor P_2 is a "limiting factor" taking into account that as the "relative flux" $\rho_2(u_2 - v)$ increases, it will become more difficult to change from lane 1 into lane 2. In the simplest case P_2 could be chosen as a characteristic function, zero above a certain critical value of the relative flux.

2.3 Discontinuous equilibria

Here we focus on the model with degenerate diffusion and explain why equilibria with discontinuities at the average speed (such as we first observed in the numerical experiments presented in Section 3 below) are to be expected. To concentrate on the essentials we consider a simplified spatially homogeneous but time-dependent model, written as

$$\partial_t f + \partial_v \mathcal{F}[f] = 0 \tag{2.11}$$

where $\mathcal{F}[f] = -(v-u)|v-u|f - |v-u|^\gamma \partial_v f$. Notice that this equation has the same fundamental structure as (1.1) with the braking/acceleration and degenerate diffusion as given above; the essential feature which was retained are the factors $|v-u|$ and $|v-u|^\gamma$; recall that $\gamma \geq 1$. We normalize the admissible speed range such that $v_{max} = 1$. To enforce the mass conservation law, Eq. (2.11) must be compemented with the no-flux boundary conditions $\mathcal{F}[f](t,0) = \mathcal{F}|f|(t,1) = 0$. In addition to this, observe that

$$\mathcal{F}[f](t,u) = 0; \tag{2.12}$$

this remains true for the more complex flux used in the full model.

For the self-consistent model under consideration we have the coupling condition $\rho u(t) = \int v f(t,v) dv$ (this is, of course, the property which makes the model nonlinear. We recall that ρ is constant by mass conservation).

If we consider for a moment the even simpler *linear* case where u in (2.11) is given and *constant*, the boundary conditions, the property (2.12), and simple integrations of (2.11) from 0 to u and from u to 1 yield that in this case $\rho_-(t) := \int_0^u f(t,v)dv$ and $\rho_+(t) := \int_u^1 f(t,v)dv$ are invariant with time; hence, there is no mass transfer through the (here prescribed) speed u, and if the solution f will converge to steady equilibria which will inherit the initial mass partitions defined by u. This will in general enforce a jump; in view of the degeneracy such discontinuous solutions are still perfectly reasonable weak solutions of Eq. (2.11).

In the nonlinear self-consistent case $u(t)$ is the average speed of f and is therefore time-dependent. Defining $\rho_-(t)$ as above one finds

$$\frac{d}{dt}\rho_- = f(t,u)\frac{du}{dt} = -\frac{d}{dt}\rho_+. \tag{2.13}$$

It is not clear from (2.13) whether or not a discontinuity will form in f as $t \to \infty$. However, it was proved in Ref. [5] that u will converge to a limit, and by (2.13) the formation of a discontinuity will be linked to the rate of convergence of u. Our numerical results in the next section suggest that u will reach a steady state so fast that insufficient mass transfer for the prevention of a discontinuity occurs, and hence the resulting equilibria have jumps.

These comments are not rigorous proofs. It is an interesting mathematical challenge to classify the initial values according to whether or not they give rise to discontinuous asymptotic states; however, we believe that residual diffusion is a reality in traffic, and therefore this challenge is largely academic.

3 Numerical experiments

3.1 The Algorithm

3.1.1 The discretization

A splitting scheme, see for example [1], is used to discretize equation (1.1). For the discretization of the first two Vlasov-type terms in equation (1.1) we use a simple first order upwind-type discretization. We note that for conservative, higher order reconstructions one could use the approach in [1]. The diffusion term is discretized in a linear-implicit way. The source terms on the right hand side are non-stiff and therefore discretized explicitly.

Zero-flux boundary conditions are used in v-space. For physical (x-space) we prescribe inflow boundary condtions at $x = x_{min}$. Due to the positive slope of the characteristics we do not need to apply boundary conditions at $x = x_{\max}$.

3.1.2 The constants

For simplicity we set

$$\rho_{\max} = u_{\max} = 1. \tag{3.14}$$

The domain is

$$x_{min} = 0, \quad x_{\max} = 10. \tag{3.15}$$

The constants for the given operators are chosen as in [6] and given by

$$\delta = 1, \gamma = 1, c_A = 5, c_B = 25, \sigma_c = 0.25. \tag{3.16}$$

In the space-dependent case we have additional constants. We take identical values for the reaction times in case of acceleration and braking

$$T_A = T_B = 0.125, H_A = H_B = 0.0375. \tag{3.17}$$

The spontaneous reaction time τ is set to $\tau = 0$ to simplify the calculations.

3.1.3 Modeling of the bottleneck

We consider a two-lane situation and use the space-dependent equations on each lane to simulate Stop- and Go-waves. We assume a restriction on road 1 in the sense that movement becomes rapidly constrained at a point $x_{\min} < x_0 < x_{\max}$. For the computations below x_0 is chosen equal to 8. We modify u^B, ρ^B and P in order to model the restriction: For points $x < x_0$ we use the formulas for ρ^B, u^B and P as given in the previous sections. Modifications are applied to u^B, ρ^B in case of

$$x + H_B + T_B v > x_0. \tag{3.18}$$

For lane 1 we set

$$u^B(x,t) = 0 \text{ and } \rho^B(x,t) = \rho_{\max} \quad \text{if } x + H_B + T_B v > x_0. \tag{3.19}$$

For lane 2 we do not change the previous definitions. The lane change probability P must be modified for both lanes for $x > x_0$. We set

$$P = \begin{bmatrix} (1-\rho_2)(x,t) \begin{bmatrix} (\frac{v-u}{u_{\max}-u})^\delta & v > u \\ 0 & \text{else} \end{bmatrix} & x \geq x_0 & \text{(in lane 1)} \\ 0 & x \geq x_0 & \text{(in lane 2)} \end{bmatrix} \tag{3.20}$$

The additional factor $(1 - \rho_2)$ prevents blow-up of the solution on road 2 due to lane changing.

3.2 The spatially homogeneous case

3.2.1 Long-term behaviour

We consider the spatially homogeneous case for smooth initial profiles and compute the emerging stationary solution as $t \to \infty$.

The constants are as in Section 3.1.2. It turns out that the final stationary solutions will in general have a discontinuity at $v = u$. (In view of our analysis in Section 2 this is to be expected). The discontinuity is robust with respect to the chosen mesh size. It remains unchanged for decreasing mesh width.

We first used a sinusoidal initial profile and computed the stationary solution; the calculation was then repeated with a linear initial profile. Both had the same density ρ, but different average speeds u. The final profiles differ, consistent with the fact observed in [6] that the fundamental diagram is multi-valued. For the results see Figures 1 and 2. We computed a two-lane situation and applied the

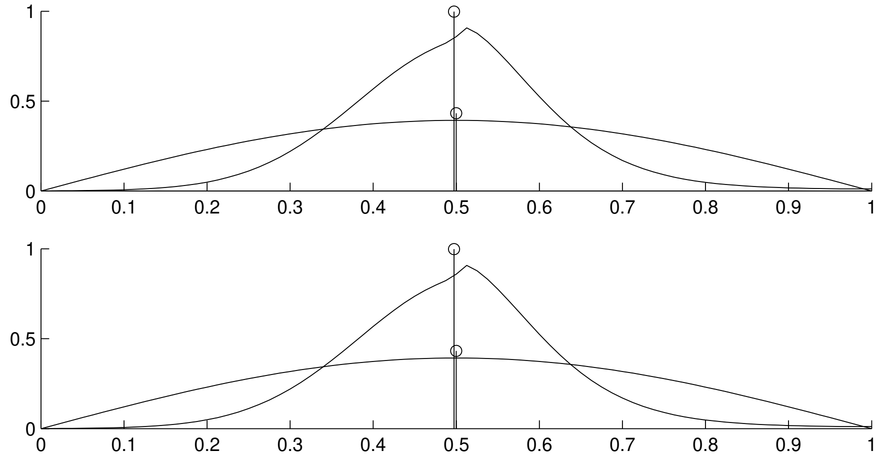

Figure 1: A sin function as an initial value. The final profile consists of two Gauss curves sparated by a discontinuity.

same initial profile to both lanes. The average velocity u is also shown in the diagrams. In all figures we plot initial and final profile in the same plot.

We present two further results on discontinuous solutions, where in both cases we start with constant initial data. The final profiles are presented in Figures 3 and 4. For the first figure we used the standard settings for the constants, i.e., $c_A = 5, c_B = 25$. For the second figure we changed the braking force to $c_A = c_B = 5$, while all other constants remain the same. We obtain a jump "down" rather than "up" with respect to the earlier example.

3.2.2 Families of discontinuous steady solutions

Recall that the equations for the spatially homogeneous case are given by

$$\begin{aligned} c_B(v-u)^2 q(\rho,u,v) f + \sigma(\rho,u)(v-u)^\gamma \partial_v f = 0 \quad v > u \\ c_A(u-v)^2(\rho_{\max}-\rho) f - \sigma(u-v)^\gamma \partial_v f = 0 \quad v < u \end{aligned} \tag{3.21}$$

Assuming $\sigma(\rho, u)$ is defined as above equation (3.21) allows solutions of the type

$$f(v) = \begin{bmatrix} c^{(2)} \exp(\beta(v-u)^{3-\gamma}[(\frac{v-u}{u_{\max}-u})^\delta \frac{1}{3-\gamma+\delta} - \frac{1}{3-\gamma}]) & v > u \\ c^{(1)} \exp(-\alpha \frac{(u-v)^{3-\gamma}}{3-\gamma}) & v < u \end{bmatrix} \tag{3.22}$$

$$\tag{3.23}$$

where $c^{(i)}$ depend on u and ρ. The functions α, β are given by

$$\alpha = \frac{c_A(\rho_{\max}-\rho)}{\sigma(\rho,u)}, \beta = \frac{c_B \rho}{\sigma(\rho,u)}. \tag{3.24}$$

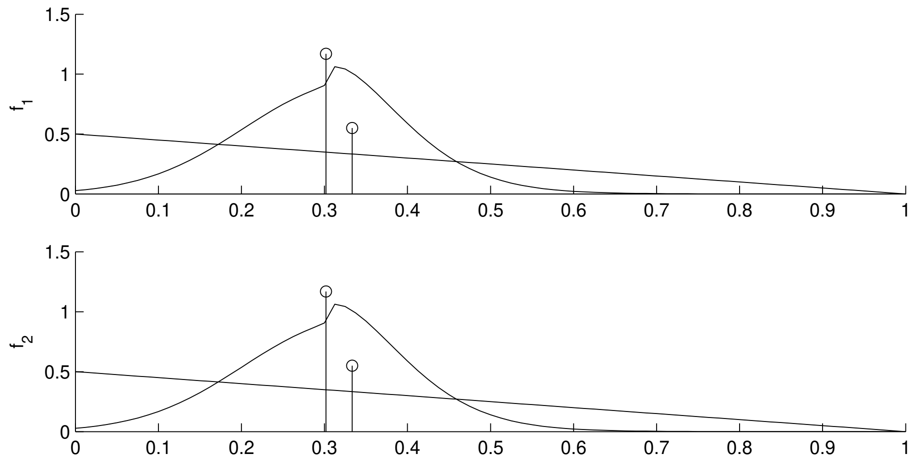

Figure 2: Linear initial profile. The final profile consists again of two Gauss curves sparated by a discontinuity.

The real-valued constants $c^{(1)}$ and $c^{(2)}$ are such that

$$\rho = \int_0^{u_{\max}} f(v)dv. \tag{3.25}$$

Hence, we obtain a one parameter family of solutions $f(v, c^{(1)}/c^{(2)})$ of equations (3.21).

We verify that the stationary solutions computed in Section 3.2.1 are of type (3.22). To this end we consider the stationary solution $\tilde{f}$ to the linear initial profile given by Figure 2 and determine constants $c^{(1)}, c^{(2)}$ by

$$\min_{c^{(1)},c^{(2)}} \|f(v, c^{(1)}/c^{(2)}) - \tilde{f}\|_\infty. \tag{3.26}$$

To compute $f(v, c^{(1)}/c^{(2)})$ we used the constants introduced in 3.1.2 and set ρ and u as in Figure 2. The stationary solution and the discontinuous solution $f(v, c^{(1)}/c^{(2)})$ for the optimal choice of $c^{(1)}/c^{(2)}$ are presented in Figure 5.

Having the one-parameter family of solutions of (3.21) we can compute a one-parameter family of fundamental diagrams by

$$\rho u = \int_0^{u_{\max}} v f(v, c^{(1)}/c^{(2)})dv, \tag{3.27}$$

i.e., for each fixed $\rho \in [0, \rho_{\max}]$ and each choice $c^{(1)}, c^{(2)}$ we compute u by the above relationship. We obtain a family of functions $u(\rho, c^{(1)}/c^{(2)})$. In Figure 6 we plot three different graphs corresponding to three choices for the quotient $c^{(1)}/c^{(2)}$. The top part of the Figure shows $u(\rho, c^{(1)}/c^{(2)})$ for the three different quotients $c^{(1)}/c^{(2)} = \{2, 1, \frac{1}{2}\}$ and varying ρ. In the lower part we plotted

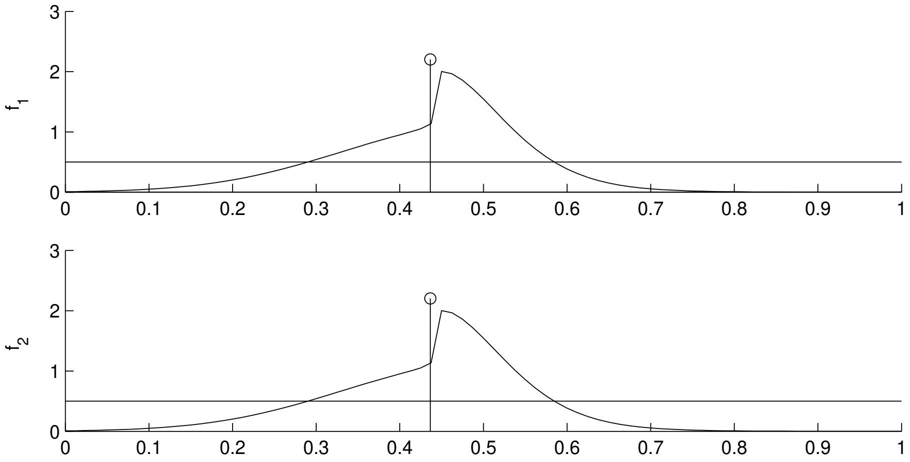

Figure 3: Constant initial profile. The final profile consists of two Gauss curvess separated by a discontinuity. c_A, c_B are as in the standard settings.

$f(v, c^{(1)}/c^{(2)})$ with the parameters $u = 0.4, \rho = \{0.3394, 0.2124, 0.1157\}$ for $c^{(1)}/c^{(2)} = \{2, 1, \frac{1}{2}\}$ respectively. Allowing discontinuous solutions as solutions of the model we obtain a region where the fundamental diagram is multivalued.

However, we emphasize that the discontinuous equilibria disappear if we insist on residual diffusion as discussed in Section 1. In this case one is left with the (still multi-valued) fundamental diagram first found in Ref. [6].

3.2.3 Synchronisation

We next investigate the question whether and how the traffic profiles on the two lanes will synchronize. Synchronization was reported by B. Kerner [9]. It is expected to be predicted by our model because of the structure of the lane changing terms on the right-hand sides. For a simplified scenario we prove in Section 4 below that synchronization must occur.

For the subsequent numerical tests we focus again on the spatially homogeneous scenario. We use the standard settings for the constants. We assume different initial profiles and look for synchronisation effects due to lane changing. First we choose a sinusoidal and a linear initial profile, see Figure 7; in a second test we take two stationary solutions with different macroscopic speed, see Figure 8. Rapid synchronization was observed in these and all other considered cases. In the appendix we present an analytical result of this type for a simplified system.

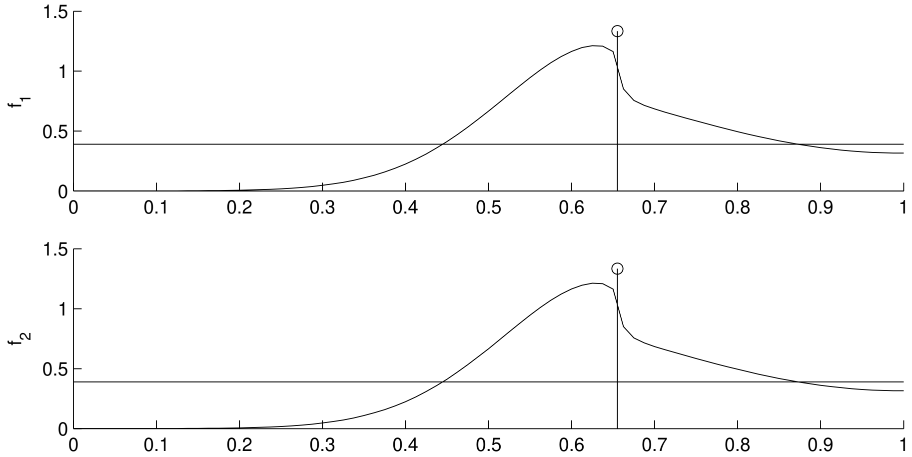

Figure 4: Constant initial profile. The final profile consists of two connected Gauss curves sparated by a disconinuity. $c_A = c_B = 5$. The other constants are as in the standard settings.

3.3 Stop-and-Go waves

This last test is concerned with a scenario where both spatial and temporal dependencies enter. We have to solve the full system, with the spatial and temporal nonlocalities taken into account.

Our objective is a reproduction of the phenomenon of stop-and-go waves as perceived behind bottlenecks on the highway. Numerical tests confirm that stop-and-go waves are produced by a trigger, like a bottleneck, the spatial nonlocalities contained in the definition of the reaction times T_B and T_A and the multi-valued fundamental diagram.

We consider two different cases with slow and fast moving traffic. In both cases stop-and-go waves are observed, and our results are given in Figure 9 and 10. We plot the averaged quantities ρ_i, j_i for fixed times t. The density

$$\rho_i(x,t) = \int_0^{u_{\max}} f_i(x,t,v)dv \qquad i = 1,2 \tag{3.28}$$

and the flux

$$j_i(x,t) = \int_0^{u_{\max}} v f_i(x,t,v)dv \qquad i = 1,2 \tag{3.29}$$

are plotted separately. We assume a bottleneck on lane one at x_0 which forces the drivers to change to lane 2. The position of the highway bottleneck is marked by a cross on the horizontal axis. We choose initial data $f_i(x,v,0)$ according to the continuous stationary solution of the Vlasov-Fokker-Planck equation, i.e.

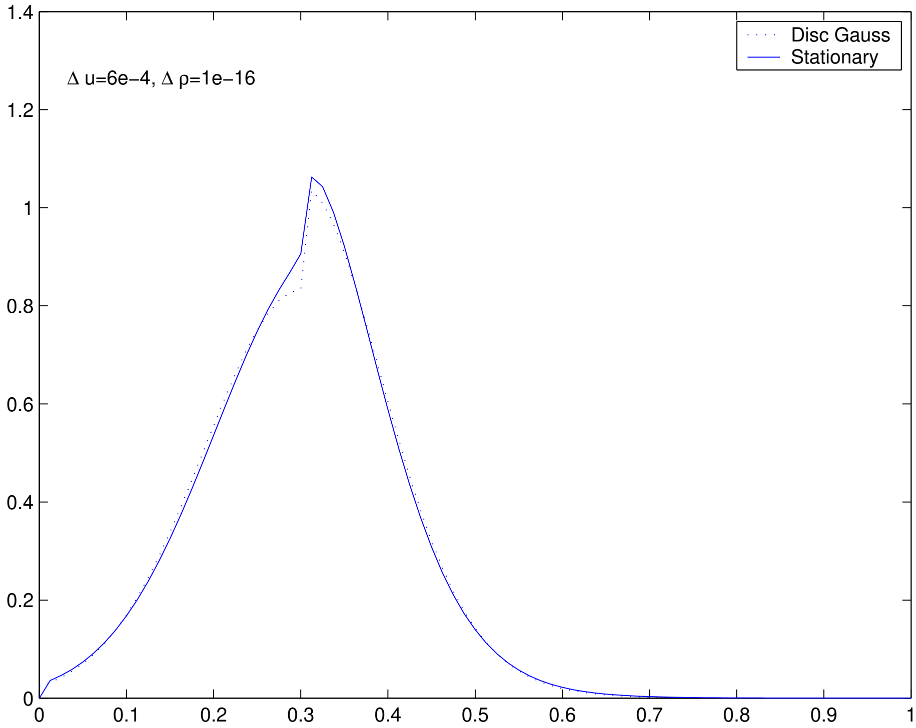

Figure 5: The asymptotic profile of a long time calculation in comparison with a stationary, discontinous Gaussian curve.

$f_i(x, v, 0)$ is chosen equal to

$$\begin{bmatrix} c(\rho(x), u(x)) \exp(\beta(v-u)^{3-\gamma}[(\frac{v-u}{1-u})^{\delta}\frac{1}{3-\gamma+\delta} - \frac{1}{3-\gamma}]) & v > u(x) \\ c(\rho(x), u(x)) \exp(-\alpha(u-v)^{3-\gamma}/(3-\gamma)) & v \leq u(x) \end{bmatrix}. \tag{3.30}$$

The constants are those given in paragraph 3.1.2. $\rho(x)$ and $u(x)$ are chosen such that for each x in the computational domain the relation

$$u(x) = \int_0^{u_{\max}} f(x, v)dv \tag{3.31}$$

holds. We set

$$x < x_0 \quad \rho(x) = \text{const}_1,\ u(x) = \text{const}_2 \tag{3.32}$$

$$x \geq x_0 \quad \rho(x) = \text{const}_3,\ u(x) = \text{const}_4 \tag{3.33}$$

where the exact values of the constants are given in Table 1 below.

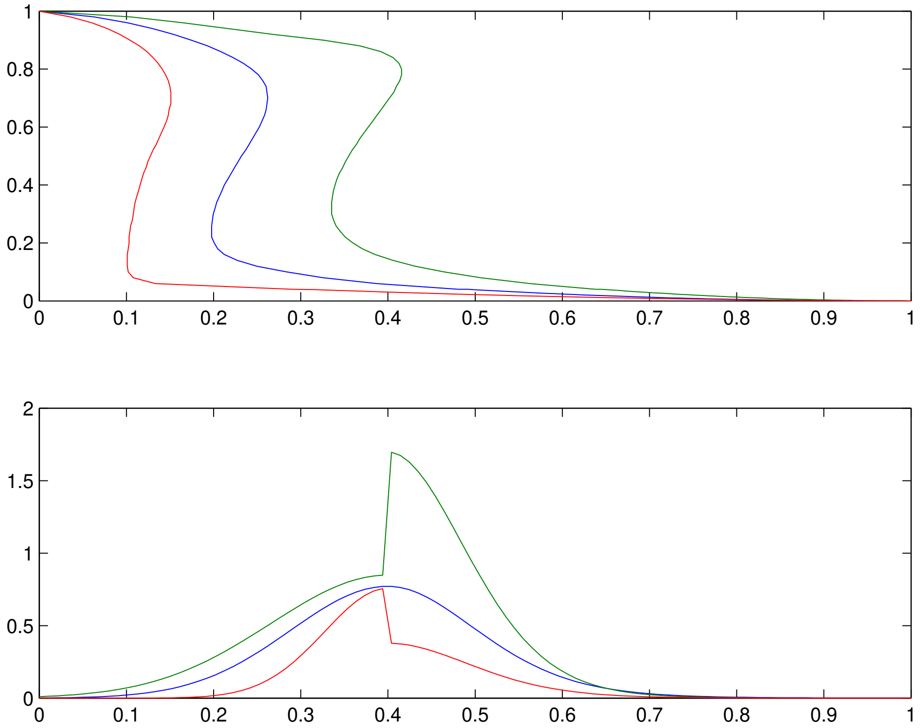

Figure 6: Fundamental diagrams and different solutions of the steady spatially homogeneous equation.

4 An analytical result on synchronization

The numerical results on synchronization from the previous section are not surprising given the nature of the lane-changing terms on the right-hand sides of the model equations. Yet, it is not a straightforward matter to prove a corresponding result analytically; if the model were a simple system of linear diffusion equations with linear exchange terms on the right hand side, synchronization could be proved by use of a variety of methods (energy or entropy methods, expansion in Fourier series, maximum principles,...), yet the self-consistent nonlinear structure of the lane changing terms, i.e., the factors j_1 and j_2 (inserted for dimensional consistency), make the adaptation of these methods challenging. We succeeded in proving synchronization nonetheless for a simplified system in which the diffusion is constant and in which braking and acceleration terms are ignored (this is, of course, not realistic, but it is a first step).

The system we consider here is thus as follows. On a highway with two lanes, assume that traffic is spatially homogeneous but has lane-dependent different velocity distributions. Will these velocity distributions synchronize as $t \to \infty$?

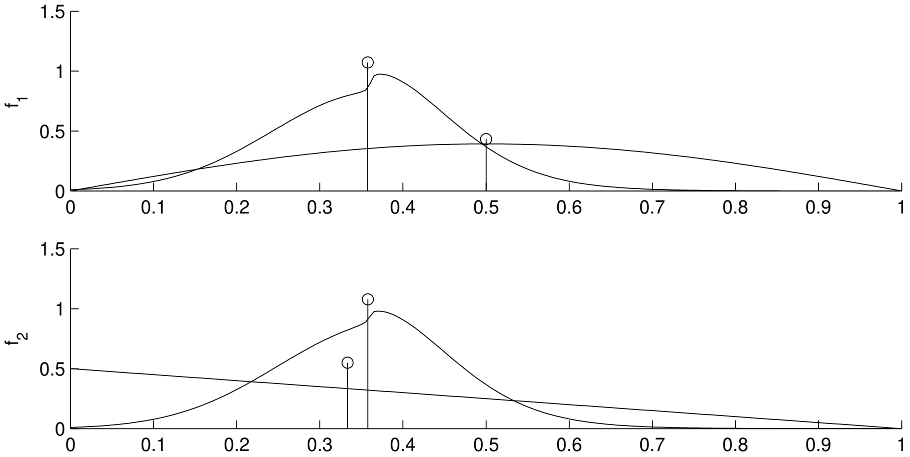

Figure 7: Sin and linear profile as initial values. The final profiles are synchronized.

Parameter	Test case 1	Test case 2
Begin of the bottleneck	$x_0 = 8$	
Number of discretization points in v	81	
Number of discretization points in x	161	
Initial density for both roads and $x < x_0$	0.2837	0.2319
Initial velocity for both roads and $x < x_0$	0.1	0.59
Initial density for both roads and $x > x_0$	0.0	
Initial velocity for both roads and $x > x_0$	1.0	

Table 1: Data for bottleneck simulation.

Our model is reduced to

$$\begin{aligned} \partial_t f_1 - \varepsilon\, \partial_v^2 f_1 &= j_2 f_2 - j_1 f_1 \\ \partial_t f_2 - \varepsilon\, \partial_v^2 f_2 &= j_1 f_1 - j_2 f_2 \end{aligned} \tag{4.34}$$

where as before $f_i = f_i(t, v)$, $i = 1, 2$, $v \in (0, 1)$, $t > 0$, and

$$j_i(t) = \int_0^1 f_i(t, v)\, v\, dv.$$

This is a simplified version of the two-lane system (1.1) in which we neglect the braking-acceleration terms and take the diffusion to be constant $\varepsilon > 0$. We shall impose the initial conditions

$$f_i(0, v) = f_{0i}(v), \quad i = 1, 2, \quad v \in (0, 1),$$

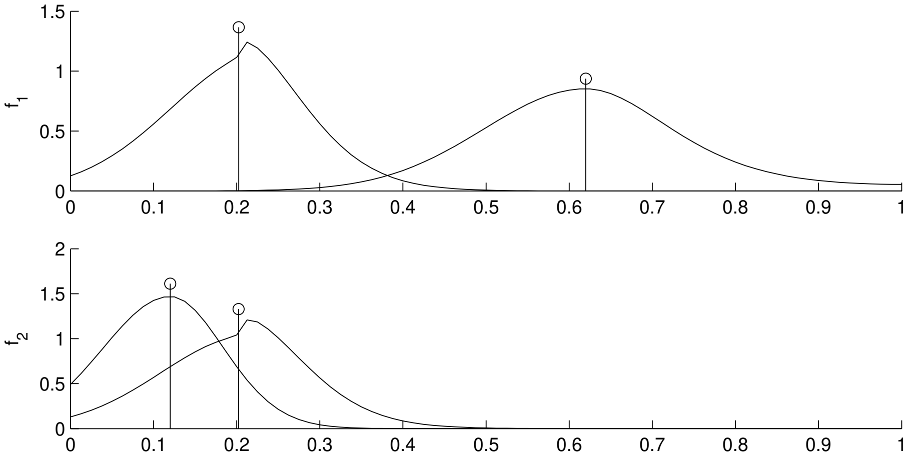

Figure 8: Two Gaussian curves with different average speeds as initial profiles, and the synchronized final profiles.

and the Neumann boundary conditions

$$\partial_v f_i(t,0) = \partial_v f_i(t,1) = 0, \quad i = 1,2, \quad t > 0,$$

which correspond to the zero-flux conditions on the boundary. It is easy to check that for $\varepsilon = 0$ the right-hand side of (4.34) has an equilibrating effect, whereas the equations with the right-hand side zero describe an exponentially fast convergence to constant steady states. However, because of the non-local dependence of the fluxes j_i on the solution, the combined result of these two effects is not immediately predictable.

We begin with some natural manipulations of the system (4.34).

First, $F = f_1 + f_2$ satisfies the equation

$$\partial_t F - \varepsilon\, \partial_v^2 F = 0 \tag{4.35}$$

with homogeneous Neumann boundary conditions. Therefore,

$$F(t,v) \to F_0 = \int_0^1 F\, dv, \quad \text{as } t \to \infty.$$

Further, setting $J(t) = \int_0^1 F\, v\, dv$ we obtain using (4.35)

$$J'(t) + (F(t,1) - F(t,0)) = 0,$$

so $J'(t) \to 0$ and $J(t) \to \int_0^1 F_0\, v\, dv = \frac{1}{2} F_0$, as $t \to \infty$.

Writing the equation for $\varphi = f_1 - f_2$ we obtain

$$\partial_t \varphi - \varepsilon\, \partial_v^2 \varphi = 2 j_2 f_2 - 2 j_1 f_1 = -F j - J \varphi,$$

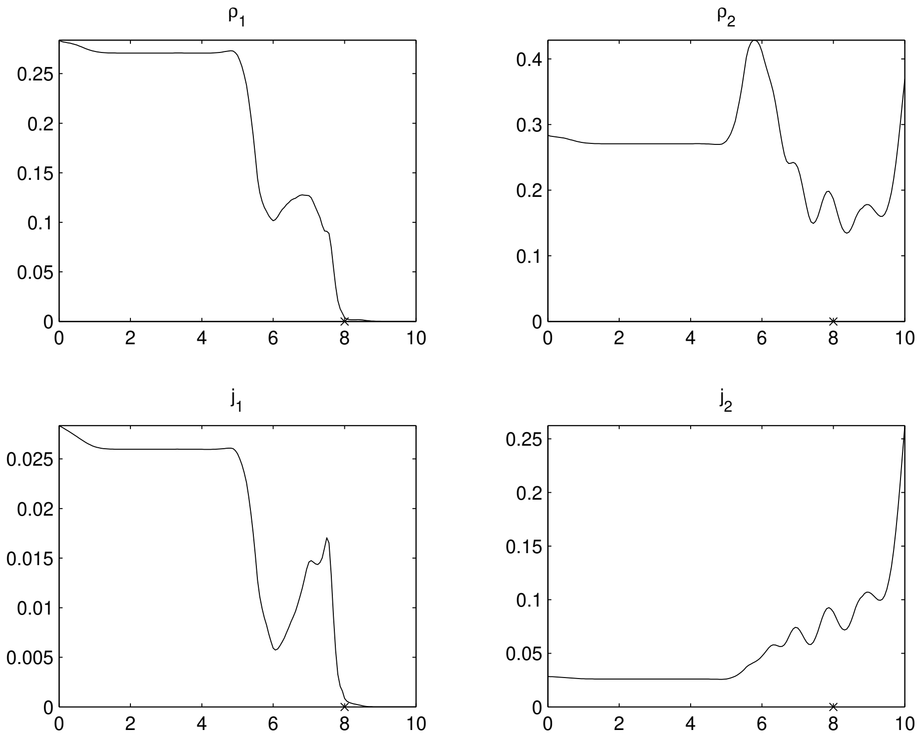

Figure 9: Intermediate profile arising during the bottleneck simulation for test case 1.

where $j = j_1 - j_2$. Multiplying the equation for φ by v and integrating we get

$$j' + 2Jj = \varepsilon(\varphi(t,0) - \varphi(t,1)).$$

Since the asymptotic behaviors of F and J are known, we replace them in the above equations by their limit values to obtain the following approximate equations:

$$\begin{cases} \partial_t \varphi - \varepsilon\, \partial_v^2 \varphi + \frac{1}{2} F_0 \varphi = -F_0 j, \\ j' + F_0 j = \varepsilon(\varphi(t,0) - \varphi(t,1)), \end{cases} \tag{4.36}$$

in which $\varphi = \varphi(t,v)$ satisfies

$$\partial_v \varphi(t,0) = \partial_v \varphi(t,1) = 0, \quad t > 0$$

and

$$j(t) = \int_0^1 \varphi\, v\, dv.$$

We now establish the following

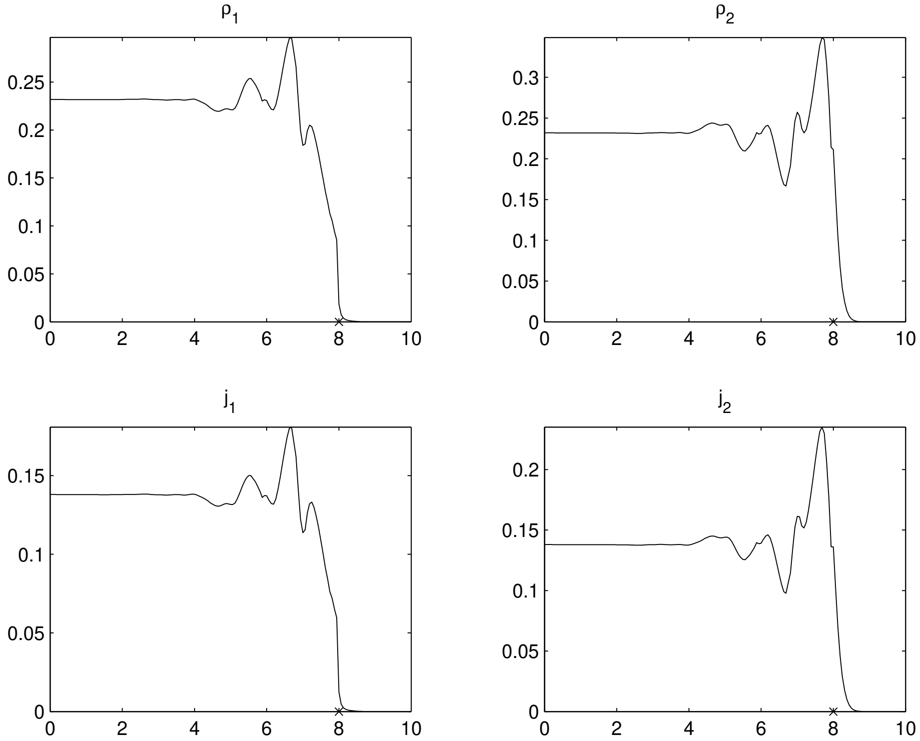

Figure 10: Intermediate profile arising during the bottleneck simulation for test case 2

Theorem 1. *For every $\varphi_0 \in L^2(0,1)$, the unique weak solution $\varphi = \varphi(t,v)$ of (4.36) satisfies*

$$\|\varphi(t,v)\|_{L^2(0,1)} \leq Ce^{-at},$$

where $C > 0$ and $a > 0$ are computable constants.

Proof. Continuing $\varphi(t,\cdot)$ to $(-1,0)$ as an even function, we can expand

$$\varphi(t,v) = \sum_{n=0}^{\infty} a_n(t)\cos(\pi n v), \tag{4.37}$$

noticing that the boundary conditions are then satisfied for any choice of $a_n(t)$. We have

$$\varphi(t,0) = \sum_{n=0}^{\infty} a_n(t) \quad \text{and} \quad \varphi(t,1) = \sum_{n=0}^{\infty} (-1)^n a_n(t),$$

so that

$$\varphi(t,0) - \varphi(t,1) = 2\sum_{n=0}^{\infty} a_{2n+1}(t).$$

Also

$$j(t) = j_0 e^{-F_0 t} + \varepsilon \int_0^t (\varphi(t,0) - \varphi(t,1))\, e^{-F_0(t-\tau)}\, d\tau,$$

where $j_0 = \int_0^1 \varphi_0\, v\, dv$. Substituting (4.37) into (4.36) we obtain the following system of equations for the Fourier coefficients:

$$a_n'(t) + \varepsilon\, \pi^2 n^2 a_n(t) + \frac{1}{2} F_0\, a_n(t) = \begin{cases} -F_0\, j(t), & n = 0 \\ 0\,, & n \neq 0 \end{cases}$$
$$j(t) = j_0\, e^{-F_0 t} + 2\varepsilon S(t).$$

where

$$S(t) = \sum_{n=0}^{\infty} \int_0^t a_{2n+1}(\tau)\, e^{-F_0(t-\tau)}\, d\tau.$$

(Notice that j is independent of v; hence it only contributes to the zero-order term on the right-hand side of the equation for a_n.)

The equations for $n \geq 1$ can be solved explicitly:

$$a_n(t) = a_n(0)\, e^{-(\varepsilon\pi^2 n^2 + \frac{1}{2} F_0)t},$$

and so we can compute

$$\int_0^t a_{2n+1}(\tau)\, e^{-F_0(t-\tau)}\, d\tau = \frac{1}{\frac{1}{2}F_0 - \varepsilon\pi^2(2n+1)^2} \left(e^{-\frac{1}{2}F_0 t - \varepsilon\pi^2(2n+1)^2)} - e^{-F_0 t} \right).$$

Thus,

$$\begin{aligned} S(t) &= e^{-\frac{1}{2}F_0 t} \sum_{n=0}^{\infty} \frac{a_n(0)}{\frac{1}{2}F_0 - \varepsilon\pi^2(2n+1)^2} e^{-\varepsilon\pi^2(2n+1)^2 t} - e^{-F_0 t} \sum_{n=0}^{\infty} \frac{a_n(0)}{\frac{1}{2}F_0 - \varepsilon\pi^2(2n+1)^2} \\ &= e^{-\frac{1}{2}F_0 t} S_1(t) + C e^{-F_0 t}, \end{aligned}$$

where $S_1(t)$ is uniformly bounded for $t > 0$. We can now use the expression for $S(t)$ to find $j(t)$ and $a_0(t)$ and obtain the exponential decay for all Fourier coefficients of φ. This completes the proof. □

While this proof does not address the synchronization question for the full traffic model, it shows at least that our lane change terms are consistent with synchronization.

Acknowledgements

This research was supported by the German Research Foundation (DFG), grant KL 1105/5, and Deutscher Akademischer Austauschdienst (DAAD), grant D/03/22853, as well as by grant No. 7847 of the Natural Sciences and Engineering Research

Council of Canada. M. Herty and A. Klar would like to thank the Department of Mathematics and Statistics at the University of Victoria, Canada, for their hospitality. V. Panferov was supported by the Pacific Institute for the Mathematical Sciences.

References

[1] F. Filbet and E. Sonnendruecker. Comparison of Eulerian Vlasov solvers. *Comp. Phys. Comm.*, 150:247–266, 2003.

[2] J. Greenberg, A. Klar, and M. Rascle. Congestion on multilane highways. *SIAM J. Appl. Math.*, 63:818–833, 2003.

[3] M. Günther, A. Klar, T. Materne, and R. Wegener. Multivalued fundamental diagrams and stop and go waves for continuum traffic flow equations. *to appear in SIAM J. Appl. Math.*

[4] D. Helbing. Gas-kinetic derivation of Navier-Stokes-like traffic equation. *Physical Review E*, 53:2366–2381, 1996.

[5] J. Dolbeault and R. Illner. Entropy methods for kinetic models of traffic flow. *Commun. Math. Sci.*, 1(3):409–421, 2003.

[6] R. Illner, A. Klar, and T. Materne. Vlasov-Fokker-Planck models for multilane traffic flow. *Comm. Math. Sci.*, 1:1–12, 2003.

[7] B.S. Kerner. Experimental features of self-organization in traffic flow. *Physical Review Letters*, 81:3797, 1998.

[8] B.S. Kerner. Congested traffic flow. *Transp. Res. Rec.*, 1678:160, 1999.

[9] B.S. Kerner. Experimental features of the emergence of moving jams in free traffic flow. *J. Phys. A*, 33:221, 2000.

[10] A. Klar and R. Wegener. Enskog-like kinetic models for vehicular traffic. *J. Stat. Phys.*, 87:91–114, 1997.

[11] A. Klar and R. Wegener. Kinetic derivation of macroscopic anticipation models for vehicular traffic. *SIAM J. Appl. Math.*, 60:1749–1766, 2000.

[12] P. Nelson and A.y Sopasakis. The Prigogine-Herman kinetic model predicts widely scattered traffic flow data at high concentrations. *Transportation Research B*, 32 A:589–604, 1998.

[13] P. Nelson. A kinetic model of vehicular traffic and its associated bimodal equilibrium solutions. *Transport Theory and Statistical Physics*, 24:383–408, 1995.

[14] S.L. Paveri-Fontana. On Boltzmann like treatments for traffic flow. *Transportation Research*, 9:225–235, 1975.

[15] I. Prigogine and R. Herman. *Kinetic Theory of Vehicular Traffic*. American Elsevier Publishing Co., New York, 1971.